



Theoretical and experimental aspects of
three-dimensional infrared photothermal
radiometry of semiconductors

メタデータ	言語: English 出版者: American Institute of Physics 公開日: 2020-06-21 キーワード: Semiconductors, Photothermal effects, Diffusion, Heat conduction, Integrated circuits 作成者: 碓, 哲雄, Salnick, Alex, Mandelis, Andreas メールアドレス: 所属:
URL	http://hdl.handle.net/10458/5279

Theoretical and experimental aspects of three-dimensional infrared photothermal radiometry of semiconductors

Tetsuo Ikari,^{a)} Alex Salnick,^{b)} and Andreas Mandelis

Photothermal and Optoelectronic Diagnostics Laboratories, Department of Mechanical and Industrial Engineering, University of Toronto, and Materials and Manufacturing Ontario, 5 King's College Road, Toronto, Ontario M5S 3G8, Canada

(Received 20 November 1998; accepted for publication 2 February 1999)

A general theoretical model for the infrared photothermal radiometric (PTR) signal from a semiconductor wafer is developed for the case of three-dimensional sample geometry with finite thickness. Carrier diffusion and heat conduction along the radial direction of the sample as well as along the thickness coordinate are taken into account. The simulated results for the modulation frequency dependence of the PTR signal amplitude and phase are applied to experimental data from Si wafers. Good agreement between the theoretical and experimental curves is obtained and several electronic and thermophysical parameters are estimated. This indicates that the three-dimensional PTR measurement is useful to remotely characterize semiconductor wafers patterned for large scale integrated circuits. © 1999 American Institute of Physics. [S0021-8979(99)01310-9]

I. INTRODUCTION

Among the physical parameters of interest, the electronic transport properties of semiconductors, namely, the carrier diffusivity, the minority carrier lifetime, and the surface recombination velocities have attracted great attention in recent semiconductor large scale integration (LSI) manufacturing. Evaluating these parameters is essential for characterizing semiconductor wafers and for modeling fabricated circuit devices on Si. Laser-induced photothermal detection techniques have been developed to monitor kinetics and transport properties of photogenerated carriers in semiconductors. Since optoelectronic behavior can be monitored in a noncontacting and nondestructive manner, these methods have advantage over conventional techniques such as frequency-dependent photoluminescence¹ or photoconductivity² methodologies. Photothermal beam deflection (PBD) and photomodulated thermoreflectance (PMTR) are the most frequently used techniques for these noncontact studies.³ The photothermal studies are based on the well-known fact that the absorption of an intensity modulated or pulsed irradiation on semiconductor results in the variation of temperature and plasma density profiles, the temporal behavior of which is affected by the thermal and electrical characteristics of the materials.

Among photothermal methodologies, infrared photothermal radiometry (PTR) has recently been under rapid development for semiconductor characterization⁴⁻¹¹ owing to its remote, noncontacting character and its potential advantages in characterizing both thermal and several electronic properties of semiconductors. PTR allows the measurement of optically induced black body radiation from the semiconductor surface. It has been shown that the frequency-domain PTR signal is extremely sensitive to the photoexcited carrier

plasma-wave in semiconductors and possesses up to five orders of magnitude higher carrier plasma-to-thermal contrast than the PMTR method.¹⁰ This fact has attracted particular attention to the PTR technique for ion implantation and device fabrication process monitoring with carrier-plasma wave technology.¹² PTR applications to ion implanted silicon wafers with qualitative analysis of the influence of thermal annealing have been reported and a preliminary quantitative experimental study has been performed on the efficiency and sensitivity of the carrier plasma wave to implantation-induced damage in Si.⁷

We have already demonstrated that the one-dimensional PTR technique is capable of characterizing ion-implantation effects on the electronic properties, as well as monitoring the contamination of Si wafers^{8,9} and Si electronic devices.^{6,7} Here, "one-dimensional" refers to the experimental configuration in which the size of the incident laser beam is large compared with the carrier plasma diffusion length. The common feature of all previous theoretical and experimental photothermal studies of semiconductors is that only homogeneous or discontinuously inhomogeneous materials have been assumed, with the exception of one published report.¹³ Correspondingly, the obtained values for carrier lifetime τ or diffusivity D usually refer to the bulk or layer characteristics of semiconductors. However, modern device processing and die sectioning requires the improvement of the spatial resolution of PTR, allowing for measurements within the scribe lines or LSI patterning on product wafers. In this paper, a general three-dimensional model for the PTR signal from semiconductor substrates is developed and compared with experimental results for Si wafers.

II. THEORETICAL MODEL

The PTR detection geometry for semiconductors has been reported earlier.⁸ The exciting laser beam is assumed to be of finite size with a Gaussian profile $\exp(-2r^2/d^2)$, is

^{a)}On leave from: Department of Electronic Engineering, Miyazaki University, Miyazaki, Japan; electronic mail: ikari@pem.miyazaki-u.ac.jp

^{b)}Current address: Therna-Wave, Inc., Fremont, California.

modulated with the angular frequency $\omega (=2\pi f)$ and focused on a laterally semi-infinite semiconductor surface. The radius of the semiconductor wafer is assumed to be sufficiently large compared with the radius of the laser beam and the detector aperture. The direction of the incident beam is normal to the surface plane. No azimuthal variation of the PTR signal is considered, i.e., the semiconductor is assumed to be isotropic thermally and electronically. The thickness of the wafer is L and the radius of the illuminating spot can be changed by using high quality lenses. The emitted infrared (IR) radiation is monitored by a fast detector focused on the excitation spot. The aperture size of the detector is finite and is also taken into account in the calculation. The present linear model is valid under the condition of carrier low injection. In our experiments, the laser power was sufficiently low to ensure the linear response of the PTR signals as a function of laser intensity.

A. The plasma-wave component

As in the development of one-dimensional PTR signal generation theory,¹² the operating mechanism involves a photoexcited carrier plasma-wave component (injected excess carrier density) and a thermal component (temperature rise). In the one-dimensional model, however, the radial spatial variation of excess carriers and temperature rise are not relevant to the calculation. In the present three-dimensional case, carrier diffusion and heat conduction along the radial direction, as well as along the axial direction in the sample are taken into account for the first time using cylindrical coordinates. A pair of conventional coupled plasma and heat diffusion equations is written and solved in Hankel space. For the plasma component of the total PTR signal, the injected three-dimensional carrier density is calculated by the following carrier transport equation:

$$\nabla^2 \Delta N(\mathbf{r}, \omega) - \sigma_n^2 \Delta N(\mathbf{r}, \omega) = -\frac{\alpha P \eta}{h \nu \pi d^2 D_n} \exp\left(-\frac{2r^2}{d^2} - \alpha z\right) \quad (1)$$

with the boundary conditions at the front and rear surface of the wafer

$$\begin{aligned} D_n \frac{\partial}{\partial z} \Delta N(r, z; \omega) \Big|_{z=0} &= s_1 \Delta N(r, 0; \omega), \\ D_n \frac{\partial}{\partial z} \Delta N(r, z; \omega) \Big|_{z=L} &= -s_2 \Delta N(r, L; \omega), \end{aligned} \quad (2)$$

where, $\sigma_n^2 = (1 + i\omega\tau_n)/D_n\tau_n$, D_n is the minority electron carrier diffusivity, τ_n is the carrier lifetime, α is the optical absorption coefficient, and s_1 and s_2 are the front and rear surface recombination velocities, respectively. P and $h\nu$ are the power and the photon energy of the incident laser beam. η is the quantum yield, which is the optical-to-electronic energy conversion efficiency.

When the energy of the exciting laser light, $h\nu$, is larger than the band-gap energy of the semiconductor, the light is strongly absorbed within a thin surface layer of the material. In this case, the absorption coefficient α does not appear explicitly in the plasma-wave equations, a phenomenon akin to photoacoustic saturation.¹⁴ The plasma-wave component

of the PTR signal is obtained from the Hankel transform $\tilde{N}(z, \lambda; \omega)$ of $N(\mathbf{r}, \omega)$, Eq. (1), by integrating over the thickness of the wafer, which takes into account deep-lying bulk Planck radiation emission from photogenerated and diffused carriers, according to Kirchhoff's law of detailed balance.¹² The result in Hankel space is

$$\begin{aligned} \tilde{F}(\lambda, \omega) &= \int_0^L \tilde{N}(z, \lambda; \omega) dz \\ &= \frac{e^{-\lambda^2 d^2/8}}{(D_n b_n + s_1) b_n} \left(\frac{A_2 + e^{-b_n L}}{A_2 - A_1 e^{-2b_n L}} \right). \end{aligned} \quad (3)$$

The collection efficiency of the IR detector can be taken into account by integrating the resulting expression over the effective aperture (or the area of A) of the detector, assuming a disk shape of radius a :

$$\begin{aligned} \tilde{S}_{\text{PTR,plasma}}(\lambda, \omega) &= \frac{1}{A} \int_0^a \tilde{F}(\lambda, \omega) J_0(\lambda \rho) \rho d\rho \\ &= \frac{1}{\pi a \lambda} \tilde{F}(\lambda, \omega) J_1(\lambda a). \end{aligned} \quad (4)$$

Finally, inverting the Hankel transform $\tilde{S}_{\text{PTR,plasma}}(\lambda, \omega)$ yields

$$S_{\text{PTR,plasma}}(\omega) = \frac{1}{\pi a} \int_0^\infty F(\lambda, \omega) J_1(\lambda a) d\lambda, \quad (5)$$

where $J_1(x)$ is the Bessel function of the first kind and of order one. The parameters in Eqs. (3) to (5) are defined as follows:

$$b_n^2 = \lambda^2 + \sigma_n^2, \quad (6)$$

$$A_1 = \frac{D_n b_n - s_1}{D_n b_n + s_1}, \quad (7)$$

$$A_2 = \frac{D_n b_n + s_2}{D_n b_n - s_2}. \quad (8)$$

B. The thermal-wave component

The thermal-wave component is also calculated in the same manner from the following coupled equation:

$$\begin{aligned} \nabla^2 \Delta T(\mathbf{r}, \omega) - \sigma_t^2 \Delta T(\mathbf{r}, \omega) + \frac{E_g}{k\tau} \Delta N(\mathbf{r}, \omega) \\ = -\frac{\alpha P \eta (h\nu - E_g)}{h \nu k \pi d^2} \exp\left(-\frac{2r^2}{d^2} - \alpha z\right), \end{aligned} \quad (9)$$

where k is the thermal conductivity, $\sigma_t^2 = i\omega/D_t$, and D_t is the sample thermal diffusivity. The heat source due to carrier relaxation to the conduction band edge and carrier band-to-band or band-to-defect recombination are included in the foregoing equations. They appear as the fourth and third term in Eq. (9), respectively. Additional heat sources at the surface boundaries are considered through the boundary conditions

$$K \frac{\partial}{\partial z} \Delta T(r, z; \omega) \Big|_{z=0} = s_1 E_g \Delta N(r, 0; \omega), \quad (10)$$

$$K \frac{\partial}{\partial z} \Delta T(r, z; \omega) \Big|_{z=L} = s_2 E_g \Delta N(r, L; \omega).$$

The PTR signal for the thermal-wave component is calculated by means of its Hankel transform as in the case of the plasma-wave component of the PTR signal, Eq. (5). The result is

$$S_{\text{PTR,thermal}}(\omega) = \frac{1}{\pi a} \int_0^\infty \tilde{G}(\lambda, \omega) J_1(\lambda a) d\lambda, \quad (11)$$

where

$$\tilde{G}(\lambda, \omega) = \int_0^L \tilde{T}(z, \lambda, \omega) dz. \quad (12)$$

After considerable algebraic manipulation, it can be shown that for strong super-band-gap absorption

$$\begin{aligned} \tilde{G}(\lambda, \omega) = & B_1 \left(\frac{1 - e^{-b_t L}}{b_t} \right) + B_2 \left(\frac{e^{b_t L} - 1}{b_t} \right) \\ & + B_3 \left(\frac{1 - e^{-b_n L}}{b_n} \right) + B_4 \left(\frac{1 - e^{-b_n L}}{b_n} \right) e^{-b_n L}. \end{aligned} \quad (13)$$

The parameters in the above equations are given as follows:

$$B_1 = \frac{h_1 - h_2 e^{-b_t L}}{1 - e^{-2b_t L}}, \quad (14)$$

$$B_2 = \left(\frac{h_1 e^{-b_t L} - h_2}{1 - e^{-2b_t L}} \right) e^{-b_t L}, \quad (15)$$

$$B_3 = - \frac{E_g e^{-\lambda^2 d^2/8}}{\pi h \nu k \tau_n (b_n^2 - b_t^2) (D_n b_n - s_1)} \left(\frac{A_2}{A_2 - A_1 e^{-2b_n L}} \right), \quad (16)$$

$$B_4 = B_3 \left(\frac{A_1}{A_2} \right), \quad (17)$$

$$\begin{aligned} h_1 = & - \frac{s_1 \tau_n}{b_t} (b_n^2 - b_t^2) (B_3 + B_4 e^{-2b_n L}) \\ & - \frac{b_n}{b_t} (B_3 - B_4 e^{-2b_n L}), \end{aligned} \quad (18)$$

$$h_2 = \frac{1}{b_t} [s_2 \tau_n (b_n^2 - b_t^2) (B_3 + B_4) - b_n (B_3 - B_4)] e^{-2b_n L}, \quad (19)$$

and

$$b_t^2 = \lambda^2 + \sigma_t^2. \quad (20)$$

The three-dimensional PTR signal is finally obtained by taking a weighted superposition of Eq. (5) and Eq. (11) to account for the plasma-wave (injected excess carrier density) and the thermal-wave (temperature rise) component, respectively. Typical variations in the PTR phase of Si wafers as a function of modulation frequency with three different spot sizes d have been calculated. Since the signal amplitude is not sensitively dependent on these physical parameters, only the phases are shown in the simulation of Fig. 1. In this

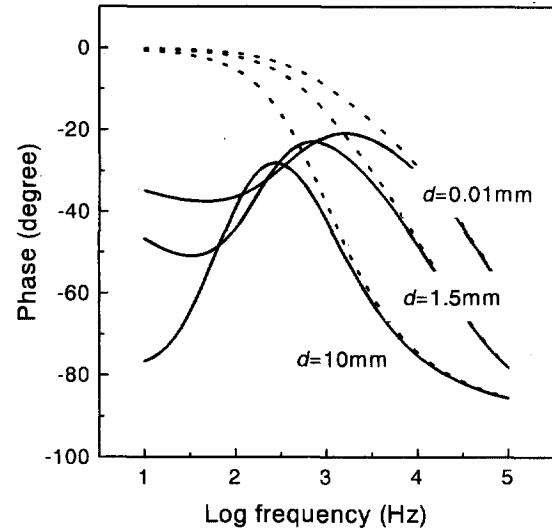


FIG. 1. Typical variations in the PTR phase of Si wafers as a function of modulation frequency with three different spot sizes d . The carrier lifetime, the carrier diffusion constant, and the surface recombination velocities on front and rear side were assumed to be 300 μs , 30 cm^2/s , 1500 cm/s , and 10⁵ cm/s , respectively. The aperture diameter of the detector and the sample thickness were set at 1 mm and 10 cm (semi-infinite), respectively. The dashed curves represent the absence of thermal-wave contributions.

calculation, we used 300 μs for the carrier lifetime, 30 cm^2/s for the n -type minority carrier diffusion constant, and 1500 and 10⁵ cm/s for the surface recombination velocities on front and rear side, respectively. The actual aperture diameter of 1 mm was used for the IR mercury cadmium telluride (MCT) detector throughout the calculations in the present paper. For the particular simulation of Fig. 1, the sample thickness was set at 10 cm (semi-infinite). The dashed and solid curves in Fig. 1 correspond to zero and finite contribution of the thermal component, respectively. Since the detector aperture diameter is 1 mm in the present case, large variations occur in the shape of the curves from one dimensional (spot size $d=10$ mm) to strongly three dimensional ($d=0.01$ mm). For the one-dimensional case where the laser beam spot size is sufficiently large compared with the aperture size of the detector, the heat conduction along the radial direction has no effect on the PTR signal generation mechanism. A similar situation prevails for carrier diffusion, as long as the diffusion length is large compared to the aperture size. Therefore, the expected curves should be the same as that reported for one-dimensional model.⁶ In the one-dimensional case, one may estimate the carrier lifetime from the turning point of the frequency dependence of the PTR signal phase. These facts indicate that care should be taken in determining the carrier lifetime by such estimation. Three-dimensional effects strongly modify the curve and the carrier lifetime is usually underestimated if the one-dimensional model is used. The recombination of diffused carriers along the radial direction renders the nominal carrier lifetime shorter than the true value, if not properly taken into account.

When the contribution of the thermal component of the PTR signal becomes large, the PTR phase decreases drastically in the lower frequency region. This lag is due to the much slower diffusion of heat than the carrier recombination.

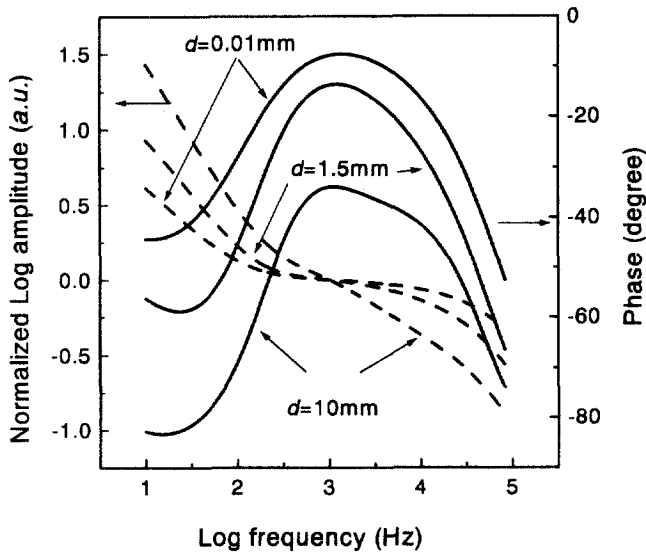


FIG. 2. Simulated PTR amplitude and the phase of a 0.5 mm thick Si wafer, the actual size for LSI applications. Carrier lifetime, electronic diffusivity, and front surface recombination velocity are the same as those in Fig. 1. The surface recombination of carriers at the rear boundary is now included in the calculation.

The thermal component does not affect the signal in the higher frequency region in both one- and three-dimensional models. The effect of the dimensionality is important to correctly analyze the PTR signal. Figure 1 overall indicates that three-dimensional effects should always be considered for estimating physical parameters such as carrier lifetime, carrier bipolar diffusion coefficient and surface recombination velocity from the frequency scan of the PTR signals.

Figure 2 shows the simulated PTR amplitude and the phase of a 0.5 mm thick Si wafer, the actual size for LSI applications. Carrier lifetime, electronic diffusivity and front surface recombination velocity are the same as those in Fig. 1. The surface recombination of carriers at the rear boundary is now included in the calculation. Both plasma- and thermal-wave terms are included in the full drawn curves. Two dominant peaks appear in the phase for the one-dimensional case of $d=10$ mm. When the beam size becomes smaller, the shoulder apparent at 10 kHz merges into a broad single peak around 1 kHz. The signal amplitude decrease becomes less steep from the one- ($d=10$ mm) to the three-dimensional case ($d=0.01$ mm). This is so because radial losses of carriers and heat contribute to signal decay throughout the entire frequency range and not only at frequencies when the carrier and thermal diffusion lengths become equal to the detector size.

III. EXPERIMENTAL RESULTS AND DISCUSSION

The detailed experimental setup for our PTR measurements has been reported earlier.¹⁰ The schematic of the apparatus is shown in Fig. 3. In the present case, the spot size of the exciting laser beam could be controlled by use of high quality optical lenses. Three typical radii of the laser beam spot size d were chosen; 0.085, 0.68, and 1.36 mm. These values were estimated by Gaussian fitting of the measured beam profile. Care was taken to keep the exciting laser

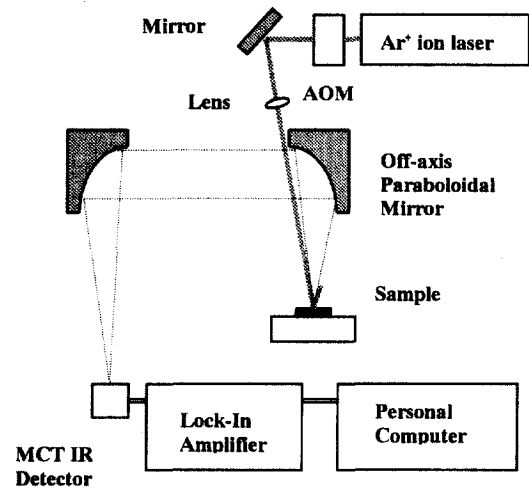


FIG. 3. Schematic setup for the experimental apparatus. The spot size of the exciting laser beam could be controlled by use of high quality optical lenses.

power low enough to obtain a linear dependence of the signal on the excitation intensity. The excitation beam was modulated from 10 Hz to 100 kHz via an acousto-optic modulator (AOM). The infrared emission was collected by two collimating off-axis paraboloidal mirrors and was focused onto a liquid nitrogen cooled HgCdTe IR detector with spectral response between 2 and 12 μm . The PTR signal from the preamplifier was fed into a lock-in amplifier and was processed by a personal computer.

Figures 4(a) and 4(b) show the observed PTR signal amplitude and phase, respectively, for a p -Si wafer. The surface of the wafer underwent oxidation in O_2/HCl , subsequent chemical etching in HF and finally was rinsed in distilled water. The experimental data were almost the same as reported earlier.⁹ No drastic change was observed by changing the beam diameter within the foregoing range of spot sizes. The curve fits of the theoretical model to the data were carried out, and the results are also shown in Fig. 4 as solid, dashed and dotted curves for laser beam spot sizes of 1.36, 0.68, and 0.086 mm, respectively. Best fitted carrier lifetime τ_n , diffusion coefficient D_n , front, s_1 , and rear, s_2 , surface recombination velocity are 200 μs , 6 cm^2/s , 50 cm/s , and 10^5 cm/s , respectively. It is noted that the plasma-wave contribution dominates the PTR signals in the entire frequency range. The ratio of thermal to plasma term became zero in this case. The long lifetime, small surface recombination velocity and small thermal wave contribution mean that this wafer was of high quality, with no significant defects or impurities near the surface region.

The observed PTR signal amplitudes and phases for an ion implanted p -Si wafer as a function of the modulation frequency are shown in Figs. 5(a) and 5(b), respectively. Phosphorous ions were implanted with an approximate dose of 10^{10} ions/ cm^2 and the implantation energy was set at 50 keV. Using the theoretical model, the experimental data shown as open squares, circles and triangles were used in a multiparameter fit. The results are shown as solid, dashed, and dotted curves for laser beam size of 1.36, 0.68, and 0.086 mm, respectively. The observed τ_n , D_n , s_1 , and s_2 of

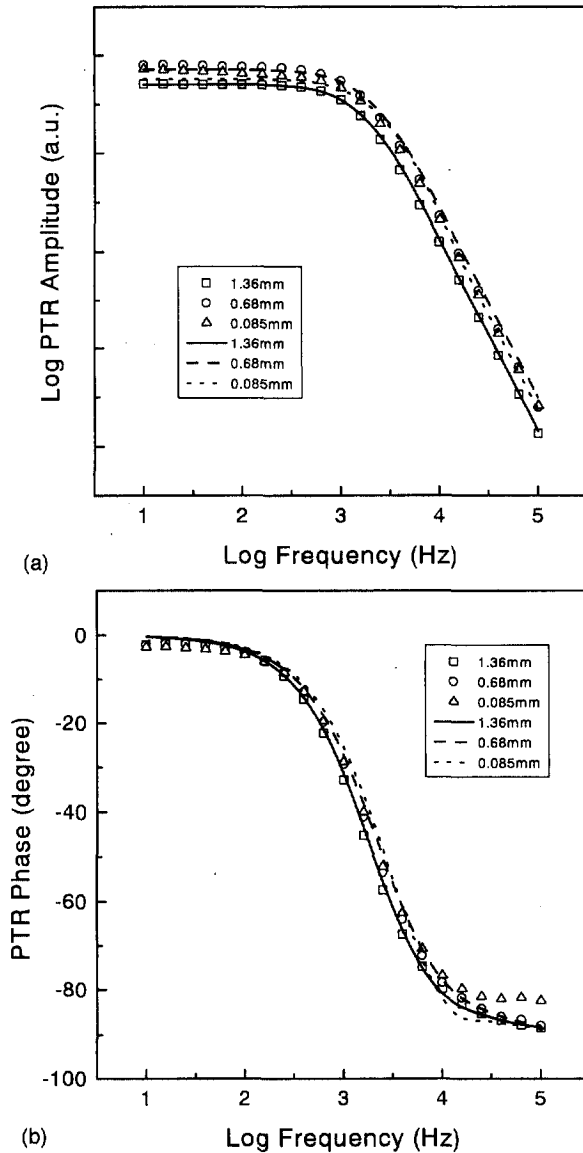


FIG. 4. Observed PTR signal (a) amplitude and (b) phase for a p-Si wafer. The surface of the wafer underwent oxidation in O_2/HCl , subsequent chemical etching in HF and finally was rinsed in distilled water. The curve fits of the theoretical model to the data are shown as solid, dashed and dotted curves for laser beam spot size of 1.36, 0.68, and 0.086 mm, respectively.

this wafer were determined to be $25 \mu s$, $100 \text{ cm}^2/\text{s}$, 1000 cm/s , and 10^5 cm/s , respectively, from the curve fitting procedure. It is seen that a considerable contribution of the thermal component appears. The thermal term was estimated to be ten times larger than that of the plasma term. Good agreement between the theory and the experiments was obtained except for the very high frequency range where depth inhomogeneities due to deep ion-implantation damage can be expected.^{10,13} Since implantation causes surface damage and generates impurities and carrier traps both in the bulk and the surface, the observed carrier lifetime decreases and surface recombination velocity increases, as expected. Although the features for the ion implanted Si wafer have already been measured,⁷ we have applied the developed three-dimensional analysis to the experimental results to obtain quantitative and

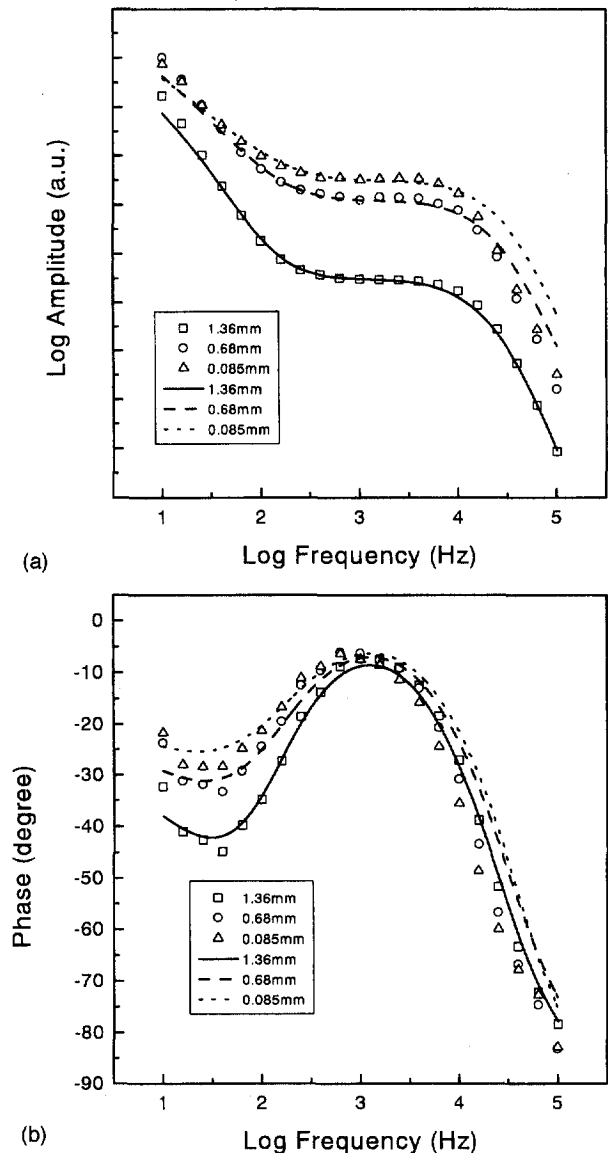


FIG. 5. Observed experimental and theoretical PTR signal (a) amplitudes and (b) phases for an ion implanted p-Si wafer as a function of the modulation frequency. Phosphorous ions were implanted with an approximate dose of $10^{10} \text{ ions/cm}^2$ and the implantation energy was set at 50 keV. Laser beam sizes were 1.36, 0.68, and 0.086 mm.

reliable estimation of the electronic parameters of Si wafers from the experimental results.

IV. CONCLUSIONS

A three-dimensional PTR signal model taking into account the finite size of the exciting laser beam, the sample thickness and both plasma- and thermal-wave contributions to the signal has been developed. The observed PTR frequency responses for Si wafers are well explained by the three-dimensional PTR model through multiparameter simultaneous fit of the PTR amplitude and phase. Carrier diffusion and heat conduction both along the radial and axial direction of the sample were taken into account simultaneously. The variations of the signal with the pump laser beam size were

also quantified. These three-dimensional measurements are quite useful for semiconductor wafers patterned for LSI circuits.

ACKNOWLEDGMENTS

The support of Materials and Manufacturing Ontario (MMO) is gratefully acknowledged. One of the authors (T.I.) also acknowledges JSPS (Japan Society for the Promotion of Science) for its support to materialize a sabbatical leave to the University of Toronto from Miyazaki University.

¹H. D. Geiler, H. Karge, M. Wagner, A. Ehlert, M. Kerstan, and D. Helmreich, *J. Appl. Phys.* **81**, 7548 (1997).

²A. Mandelis, A. Othonos, C. Christofides, and J. Boussey-Said, *J. Appl. Phys.* **80**, 5332 (1996).

³*Photoacoustic and Thermal-Wave Phenomena in Semiconductors*, edited by A. Mandelis (North-Holland, Amsterdam, 1987).

⁴S. Sheard and M. Somekh, in *Non-destructive Evaluation (Progress in Photothermal and Photoacoustic Science and Technology Vol. 2)*, edited by A. Mandelis (Prentice-Hall, Englewood Cliffs, NJ, 1994), p. 111.

⁵A. Mandelis, R. Bleiss, and F. Shimura, *J. Appl. Phys.* **74**, 3431 (1993).

⁶A. Mandelis, A. Othonos, C. Christofides, and J. Boussey-Said, *J. Appl. Phys.* **80**, 5332 (1996).

⁷Salnick, A. Mandelis, F. Funak, and C. Jean, *Appl. Phys. Lett.* **71**, 1531 (1997).

⁸A. Salnick, C. Jean, and A. Mandelis, *Solid-State Electron.* **41**, 591 (1997).

⁹A. Salnick, A. Mandelis, and C. Jean, *Phys. Status Solidi A* **163**, R5 (1997).

¹⁰A. Salnick, A. Mandelis, H. Ruda, and C. Jean, *J. Appl. Phys.* **82**, 1853 (1997).

¹¹C. Christofides, *Semiconductors and Semimetals*, edited by R. K. Willardson and E. R. Weber (Academic, New York, 1997), Vol. 46, p. 115.

¹²A. Mandelis, *Solid-State Electron.* **42**, 1 (1997).

¹³A. Salnick and A. Mandelis, *J. Appl. Phys.* **80**, 5278 (1996).

¹⁴A. Rosencwaig and A. Gersho, *J. Appl. Phys.* **47**, 64 (1976).